Anodic Electrodeposition of Nanocrystalline Coatings in the Mn−Co−O System

Weifeng Wei,* Weixing Chen, and Douglas G. Ivey

Department of Chemical and Materials Engineering, University of Alberta, Edmonton, Alberta, Canada T6G 2G6

Received January 16, 2007. Revised Manuscript Received March 12, 2007

Nanocrystalline coatings in the Mn−Co−O system have been anodically electrodeposited on ferritic stainless steel substrates from aqueous solutions. A range of Co/Mn compositions (20−65 atom % Co) can be deposited by adjusting the deposition parameters, i.e., solution temperature, metal ion concentration and current density. Electron microscopy analysis shows that the coatings are composed of numerous oxide grains (less than 10 nm in diameter), which have a metastable face center cubic (FCC) structure. The crystal structure of as-deposited coatings is not sensitive to deposition parameters. The effects of deposition parameters on coating morphology have also been investigated. Crack formation in Mn−Co−O coatings depends on process conditions, but is not related to phase structure, grain size, or even coating composition.

Introduction

The advent of an anode-supported planar solid oxide fuel cell (SOFC) design allows SOFC stacks to operate at intermediate temperature (≤800 °C). In an anode-supported SOFC, a very thin electrolyte (<20 μm thick) is used in the planar configuration to reduce the ohmic resistance contributing to the overall cell voltage loss.[1−5] This anode-supported concept, in principle, allows a $LaCrO_3$-based ceramic interconnect to be replaced by a metallic interconnect due to the reduction of the operating temperature. Iron-based alloys, especially ferritic stainless steels, are among the most promising materials for interconnects in SOFCs because of their many advantages over doped $LaCrO_3$ ceramics, Cr-based alloys, and Ni-based alloys. These advantages include good mechanical properties, reasonable thermal and electronic conductivity, ease of fabrication, and much lower cost. However, high growth rates and volatility of the chromia scale are the two main drawbacks for Cr-containing iron-based alloys.[6−7] Rapid growth of the chromia scale leads to high contact resistance and in turn deteriorates the cell performance. Volatile Cr species from the chromia scale can rapidly poison the cathode or the cathode-electrolyte interface. One way of overcoming these shortcomings is through the application of a Cr-free protective coating on Cr-containing iron-based alloys.

Manganese cobalt oxides ($Mn_xCo_{3-x}O_4$ with $0 < x < 3$) constitute a group of materials that have been widely studied by many investigators:[8−13] A cubic *Fd*3*m* spinel-type solid solution is formed in the compositional range of $x < 1.4$, with the cell lattice parameter ranging from 0.8076 nm for Co_3O_4 ($x = 0$) to 0.8321 nm ($x = 1.4$). A tetragonal (space group $I4_1/amd$) single phase is formed in the interval $2.0 < x < 3.0$. Materials with $1.4 < x < 2.0$ are mixtures of cubic and tetragonal spinel-type phases. Recently, Mn−Co spinel oxides have been introduced as protective coatings for ferritic stainless steel interconnects in SOFCs because of their higher electronic conductivity,[14−17] better chemical stability and compatibility,[14−19] and lower thermal expansion

* To whom correspondence should be addressed. E-mail: weifeng@ualberta.ca.

(1) Kabs, H.; Stimming, U.; Stovers, D. *Proceedings of the Fifth International Symposium on Solid Oxide Fuel Cells*, Aachen, Germany, June 1997; The Electrochemical Society: Pennington, NJ, 1997; pp 160−170.
(2) Foger, K.; Donelson, R.; Ratnaraj, R. *Proceedings of the Sixth International Symposium on Solid Oxide Fuel Cells*, Honolulu, Hawaii, October 1999; The Electrochemical Society: Pennington, NJ, 1999; pp 95−100.
(3) DeHaart, L. G. J.; Vinke, I. C.; Janke, A.; Ringel, H.; Tietz, F. *Proceedings of the Seventh International Symposium on Solid Oxide Fuel Cells*, Tsukuba, Ibaraki, Japan, June 2001; The Electrochemical Society: Pennington, NJ, 2001; pp 111−119.
(4) Yasuda, I.; Baba, Y.; Ogiwara, T.; Yakabe, H.; Matsuzaki, Y. *Proceedings of the Seventh International Symposium on Solid Oxide Fuel Cells*, Tsukuba, Ibaraki, Japan, June 2001; The Electrochemical Society: Pennington, NJ, 2001; pp 131−139.
(5) Kim, J. W.; Virkar, A. V.; Fung, K. Z.; Mehta, K.; Singhal. S. C. *J. Electrochem. Soc.* **1999**, *146*, 69−78.
(6) Badwal, S. P. S.; Deller, R.; Foger, K.; Ramprakash, Y.; Zhang, J. P. *Solid State Ionics* **1997**, *99*, 297−310.
(7) Matsuzaki, Y.; Yasuda, I. *Solid State Ionics* **2000**, *132*, 271−278.
(8) Naka, S.; Inagaki, M.; Tanaka, T. *J. Mater. Sci.* **1972**, *7*, 441−444.
(9) Jimenez-Mateo, J. M.; Morales, J.; Tirado, J. L. *J. Solid State Chem.* **1989**, *82*, 87−94.
(10) Martin de Vidales, J. L.; Garcia-Martinez, O.; Vila, E.; Rojas, R. M.; Torralvo, M. J. *MRS Bull.* **1993**, *28*, 1135−1143.
(11) Rojas, R. M.; Vila, E.; Garcia-Martinez, O.; Martin de Vidales, J. L. *J. Mater. Chem.* **1994**, *4*, 1635−1639.
(12) Martin de Vidales, J. L.; Vila, E.; Rojas, R. M.; Garcia-Martinez, O. *Chem. Mater.* **1995**, *7*, 1716−1721.
(13) Vila, E.; Rojas, R. M.; Martin de Vidales, J. L.; Garcia-Martinez, O. *Chem. Mater.* **1996**, *8*, 1078−1083.
(14) Yang, Z. G.; Xia, G. G.; Simner, S. P.; Stevenson, J. W. *J. Electrochem. Soc.* **2005**, *152*, A1896−A1901.
(15) Yang, Z. G.; Xia, G. G.; Simner, S. P.; Stevenson, J. W. *Electrochem. Solid-State Lett.* **2005**, *8*, A168−A170.
(16) Chen, X.; Hou, P. Y.; Jacobson, C. P.; Visco, S. J.; De Jonghe, L. C. *Solid State Ionics* **2005**, *176*, 425−433.
(17) Huang, K.; Hou, P. Y.; Goodenough, J. B. *Solid State Ionics* **2000**, *129*, 237−250.
(18) Larring, Y.; Norby, T. *J. Electrochem. Soc.* **2000**, *147*, 3251−3256.
(19) Qu, W. Interconnect Coatings for Solid Oxide Fuel Cell Applications. Masters Thesis, University of Calgary, Calgary, Alberta, Canada, 2004.

10.1021/cm070147q CCC: $37.00
Published on Web 04/27/2007

mismatch compared with chromia and Cr-containing oxide coatings.[16,19] Typical preparation methods are slurry spraying,[14,16] screen printing,[15] and sol−gel processing,[19] based on cobalt and manganese oxide mixtures, followed by solid-state reaction at high temperatures.

Electrochemical deposition has several distinct advantages for the preparation of thin film materials.[20] The low processing temperatures (often room temperature) of electrochemical deposition minimize interdiffusion. In addition, uniform films can be deposited on substrates of complex shape with a high degree of reproducibility and film thickness can be precisely controlled by simply changing the delivered electrical charge. The composition and defect chemistry can be controlled through the applied overpotential and the technique setup is not capital intensive. Anodic electrooxidation has been widely employed to obtain metal oxide deposits by directly oxidizing soluble species in a lower oxidation state to insoluble species in a higher oxidation state. Examples are the synthesis of MnO_2 from Mn^{2+} solutions,[21] Bi_2O_3 from Bi^{3+} solutions,[22] Co_3O_4 from Co^{2+} solutions,[23] and binary Tl−Pb,[24−25] Co−Ni,[26] Co−Fe,[27] Co−Mn,[28] and Ni−Mn[29] oxides from Tl^{2+}/Pb^{2+}, Co^{2+}/Ni^{2+}, Co^{2+}/Fe^{2+}, Co^{2+}/Mn^{2+}, and Ni^{2+}/Mn^{2+} solutions, respectively.

Transition metal oxide coatings using anodic electrodeposition, such as Co−Mn and Ni−Mn oxide coatings, may develop cracks after deposition. The exact reasons for crack formation on oxides coatings are unknown. Homogeneously distributed cracks are beneficial for oxide coatings used for capacitive properties.[28−29] However, homogeneous cracks are detrimental to high-temperature oxidation-resistant coatings, because the penetration of oxygen to the substrates is favored by the presence of cracks. Another difficulty in developing Co−Mn oxide coatings is that Mn oxides are preferentially deposited even when the Co/Mn molar ratio in the electrodepostion solutions is high.[28] Mn-rich, Mn−Co−O coatings have lower electrical conductivities and higher thermal expansion coefficient differences when compared with their Co-rich counterparts.[16−18] Therefore, the development of crack-free, conductive Mn−Co oxide coatings with high Co contents is important for application to metallic interconnects in SOFCs.

The purpose of this work is to anodically electrodeposit Co-rich, Mn−Co−O coatings without cracks on ferritic stainless steel substrates directly from aqueous solutions. The electrodeposition process and the effects of experimental parameters, including solution temperature, metal ion concentration, and current density, on the morphology, chemistry, and structure of as-deposited Mn−Co−O coatings are also discussed.

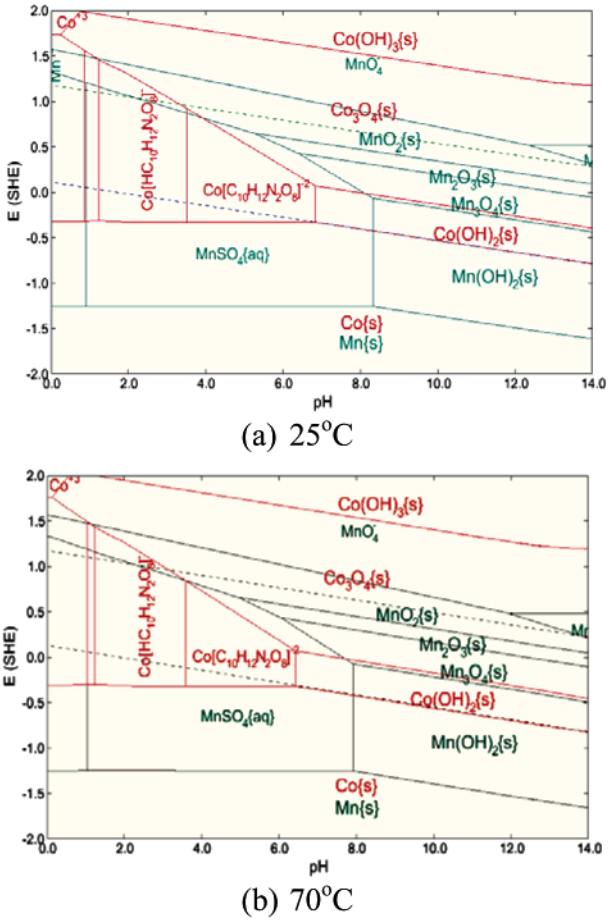

Figure 1. Calculated Pourbaix diagrams for 0.2 M EDTA solutions with 0.27 M $CoSO_4 \cdot 7H_2O$ + 0.03 M $MnSO_4 \cdot 7H_2O$ at (a) 25 and (b) 70 °C.

Experimental Section

The Mn−Co−O coatings were anodically electrodeposited on ferritic stainless steel substrates with dimensions of 20 mm × 10 mm × 1mm using a Gamry PC4/750 potentiostat/galvanostat. The solutions consisted of 0.2 M EDTA disodium and various concentrations of $CoSO_4 \cdot 7H_2O$ and $MnSO_4 \cdot 7H_2O$. Four different Co(II)/Mn(II) mole ratios, 3:1, 9:1, 29:1, and 59:1, were used and the total metal ion concentration was set to 0.3 M. EDTA disodium was applied to stabilize the solutions. The solution pH was maintained in the 5.6−6.0 range. A three-electrode cell configuration was used and consisted of a platinum counter electrode placed horizontally 20 mm above a horizontal stainless steel working electrode. A saturated calomel electrode (SCE) was used as the reference and all the potentials quoted are with respect to it. Before anodic deposition, the steel substrates were ground with 600-grit SiC abrasive papers, degreased in an alkaline solution at 80 °C, and cleaned ultrasonically in deionized water. The steel substrates were anodically activated at a current density of 30 mA/cm^2 for 2 min in a 0.2 M H_2SO_4 solution and then cathodically activated at a current density of 30 mA/cm^2 for 6 min in a 0.1 M HCl solution. The aims of the activation processes were to remove the native oxide film and to obtain rough, clean surfaces on the stainless steel substrates to improve the adhesion properties of the Mn−Co−O coatings. The Mn−Co−O coatings were prepared on the activated steel substrates under galvanostatic control with current densities

(20) Hodes, G. *Electrochemistry of Nanomaterials*; Wiley-VCH: Weinheim, Germany, 2001; pp 67−101.
(21) Preisler, E. *J. Appl. Electrochem.* **1989**, *19*, 540−546.
(22) Switzer, J. A.; Shumsky, M. G.; Bohannan, E. W. *Science* **1999**, *284*, 293−296.
(23) Nakaoka, K.; Nakayama, M.; Ogura, K. *J. Electrochem. Soc.* **2002**, *149*, 159−163.
(24) Switzer, J. A.; Shane, M. J.; Phillips, R. J. *Science* **1990**, *247*, 444.
(25) Phillips, R. J.; Golden, T. D.; Shumsky, M. G.; Bohannan, E. W.; Switzer, J. A. *Chem. Mater.* **1997**, *9*, 1670.
(26) Wu, G.; Li, N.; Zhou, D. R.; Mitsuo, K.; Xu, B. Q. *J. Solid State Chem.* **2004**, *177*, 3682−3692.
(27) Sartale, S. D.; Lokhande, C. D. *Ceram. Int.* **2002**, *28*, 467−477.
(28) Chuang, P. Y.; Hu, C. C. *Mater. Chem. Phys.* **2005**, *92*, 138−145.
(29) Chen, Y. S.; Hu, C. C. *Electrochem. Solid-State Lett.* **2003**, *6*, A210−A213.

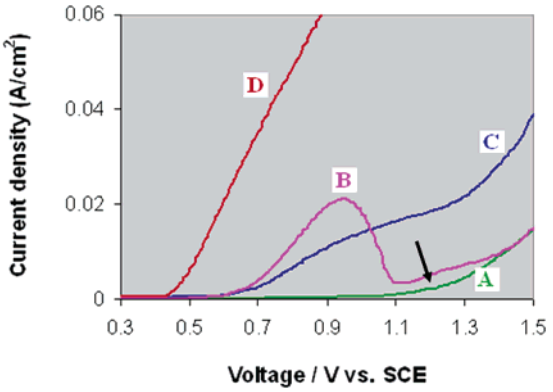

Figure 2. Linear sweep voltammetry for 0.2 M EDTA solutions with (A) 0.27 M $CoSO_4 \cdot 7H_2O$ at 25 °C, (B) 0.27 M $CoSO_4 \cdot 7H_2O$ + 0.03 M $MnSO_4 \cdot 7H_2O$ at 25 °C, (C) 0.27 M $CoSO_4 \cdot 7H_2O$ at 70 °C, and (D) 0.27 M $CoSO_4 \cdot 7H_2O$ + 0.03 M $MnSO_4 \cdot 7H_2O$ at 70 °C. The scan rate was 5 mV/s.

ranging from 5 to 50 mA/cm^2. During electrodeposition, agitation was introduced with a magnetically driven Teflon-coated stirring bar at a speed of 300 rpm.

After electrodeposition, the working electrodes were rinsed with deionized water and dried in air. Preliminary examination of deposited samples was done through thin film X-ray diffraction (XRD), using a Rigaku rotating Co anode system (40 kV, 160 mA) operating in the step scanning mode. The morphology and chemistry were analyzed in a Hitachi S-2700 scanning electron microscope (SEM), equipped with an ultrathin window (UTW) X-ray detector, and a JAMP 9500F scanning Auger microprobe. A JEOL 2010 transmission electron microscope (TEM), equipped with a UTW X-ray detector, was applied to study the microstructure and composition of the coatings at higher magnification. Crystal structure analysis was performed using selected area diffraction (SAD) patterns.

Plan view samples for TEM analysis were first ground to a final thickness of ~30 μm from the uncoated steel side using 400- and 600-grit SiC abrasive papers. The samples were then polished using 3 and 1 μm diamond polishing pastes. The polished samples were sputtered from the uncoated side to perforation in an ion mill using an Ar^+ beam operating at an energy of 6 kV with a current of 0.5 mA and an incidence angle of 17° to the surface. All samples were cooled with liquid nitrogen during sputtering to reduce preferential sputtering effects. After perforation, the sputtering angle was decreased to 13° and the current and gun energy were lowered to 0.3 mA and 3.5 kV, respectively, for an additional 30 min.

Results and Discussion

Electrochemical Processing. The electrochemical process in anodic deposition can be thermodynamically evaluated through stability diagrams (Pourbaix diagrams). Pourbaix diagrams with multiple components and complexing agents are not available in the literature. In this research work, Pourbaix diagrams were calculated with OLI Analyzer version 2.1 software purchased from OLI Systems, Inc. Panels a and b of Figure 1 are calculated Pourbaix diagrams for a solution with a Co(II)/Mn(II) molar ratio of 9:1 at 25 and 70 °C, respectively. From the two diagrams, it is apparent that the solution is stable at a pH of 6.0 and Co(II) should be oxidized at a lower potential when compared with Mn-(II) ions, which means cobalt oxides should deposited preferentially from a thermodynamic perspective. An increase in temperature has a negligible influence on the electrooxi-

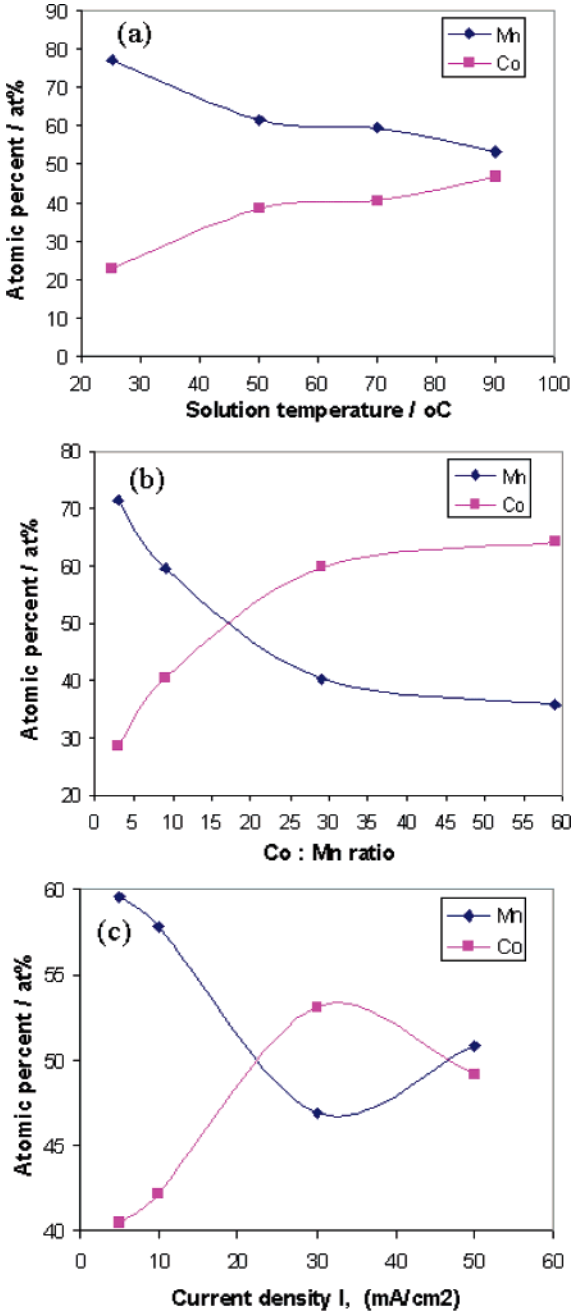

Figure 3. Effect of deposition parameters on Mn−Co−O coating composition. (a) Effect of solution temperature. Electrodeposition was conducted at 5mA/cm^2 from solutions containing a 9:1 Co:Mn ratio. (b) Effect of solution Co:Mn ratio. The solution temperature was maintained at 70 °C and the current density was 5 mA/cm^2. (c) Effect of current density. The solution temperature was maintained at 70 °C and solution Co:Mn ratio was 9:1.

dation potentials of both Co(II) and Mn(II) ions, but slightly reduces the size of the stable zones for Co(II) and Mn(II) ions.

Linear sweep voltammetry (LSV) curves for 0.2 M EDTA solutions containing 0.27M $CoSO_4 \cdot 7H_2O$ or 0.27 M $CoSO_4 \cdot 7H_2O$ + 0.03 M $MnSO_4 \cdot 7H_2O$, obtained at 25 and 70 °C, are compared in Figure 2. Curve A shows the linear sweep with no Mn(II) ions in the Co(II) solution at 25 °C. No distinct anodic current related to the oxidation of Co(II) is present except for electrogeneration of oxygen starting at ~1.2 V vs SCE, shown with an arrow in Figure 2. The addition of 0.03 M Mn(II) ions in the Co(II) solution leads

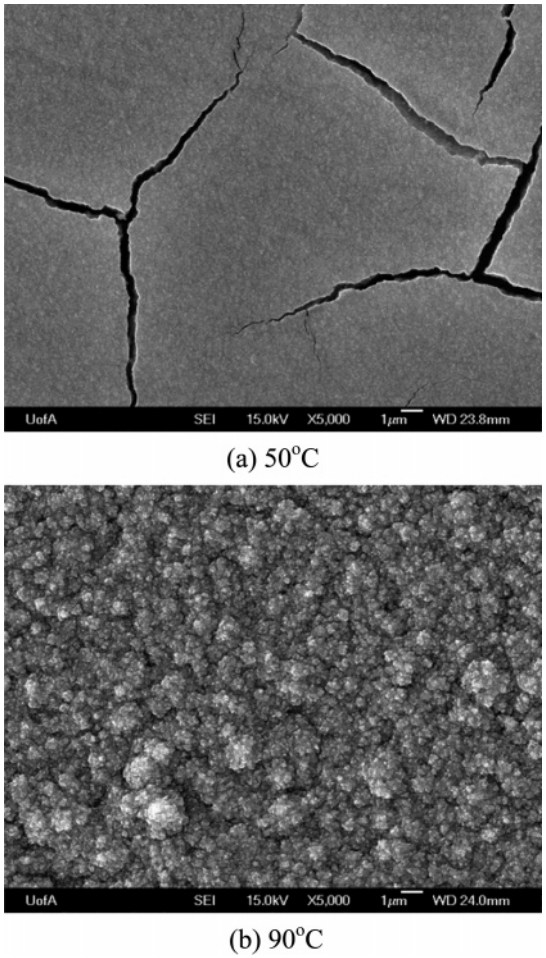

Figure 4. Plan view SEM images of Mn−Co−O coatings prepared from a 0.27 M $CoSO_4$ + 0.03 M $MnSO_4$ solution at a temperature of (a) 50 and (b) 90 °C. The deposition current density was 5 mA/cm^2.

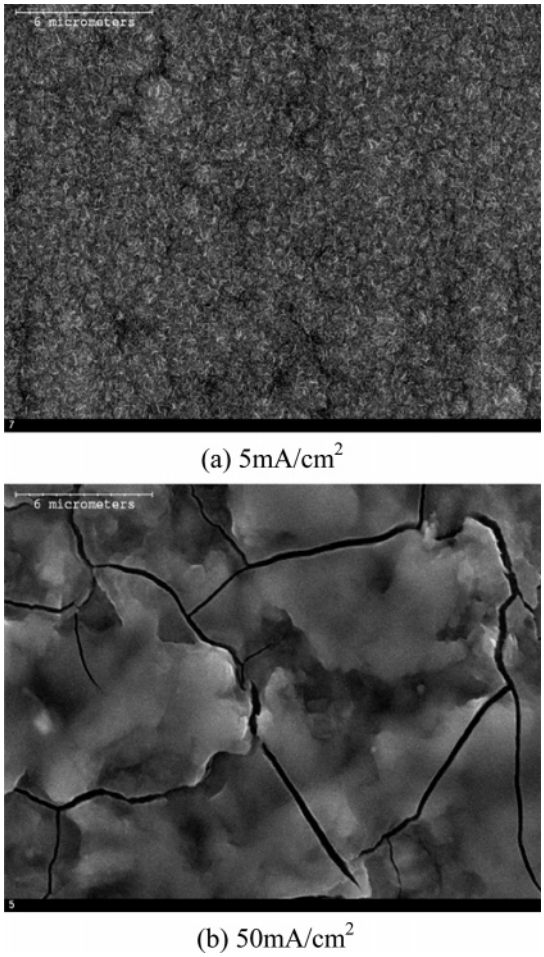

Figure 5. Plan view SEM images of Mn−Co−O coatings prepared from a 0.27 M $CoSO_4$ + 0.03 M $MnSO_4$ solution at 70 °C with current densities of (a) 5 and (b) 50 mA/cm^2.

to a distinct current rise with an onset potential of ∼0.6 V vs SCE, as shown in curve B. The electrooxidation onset potentials are determined on the basis of extrapolation from the large linear sections at high current to the voltage axis. Curves C and D are LSV spectra of Co(II) solutions with and without Mn(II) ions at a temperature of 70 °C, respectively. As solution temperature increases, the onset potentials shift to the cathodic direction, and the current densities rise rapidly in the Co(II) solutions with and without Mn(II) ions. Electrooxidation of Mn(II) ions to higher valence oxides is much more rapid than electrooxidation of Co(II) ions, even when the Co(II) /Mn(II) molar ratio is 9:1 in the solution. A possible explanation for the sluggish reaction of Co(II) could be attributed to the extremely low dissociation constant (K_d) of cobalt sulfate heptahydrate in solution. From the HSC Chemistry 5.11 database,[30] the K_d of cobalt sulfate heptahydrate at 20 °C is 4.831×10^{-24}, whereas it is 5.560 for manganese sulfate heptahydrate under the same conditions. This may explain the discrepancy between theoretical prediction based on Pourbaix diagrams and the actual LSV spectra. As the solution temperature increases to 70 °C, the K_d of cobalt sulfate heptahydrate is more than 3 orders of magnitude higher than that obtained at room temperature.[30] Meanwhile, the K_d of manganous sulfate heptahydrate increases by about 40% at 70 °C.[30] Although the K_d of cobalt sulfate heptahydrate is still very low at high temperature, the combination of high solution temperature and high Co/Mn molar ratio in the solutions can be an effective way to solve the problem of preferential deposition of Mn oxides.

Deposit Chemistry. The effect of deposition parameters on the composition of Mn−Co−O coatings is shown in Figure 3. Figure 3a shows how solution temperature affects the Mn−Co−O coating composition. Cobalt content in the coatings increases steadily with increasing solution temperature, almost doubling as the solution temperature is raised from 25 to 90 °C. The results are not predicted using calculated Pourbaix diagrams, but agree well with the LSV spectra shown in Figure 2. This means that high solution temperatures kinetically favor the deposition of Co oxides. Figure 3b demonstrates the effect of solution Co:Mn ratio on Mn−Co−O coating composition. Here, the solution temperature was maintained at 70 °C. Higher Co contents were obtained at higher Co:Mn ratios, with deposit Co composition reaching a maximum of about 60 at %. This also correlates to the kinetics of the deposition process. The effect of current density on the composition of Mn−Co−O coatings is illustrated in Figure 3c. The solution temperature was maintained at 70 °C and the Co:Mn solution composition

(30) Roine, A. *HSC Chemistry 5.11 software*; Outokumpu Research Oy: Pori, Finland, 2002.

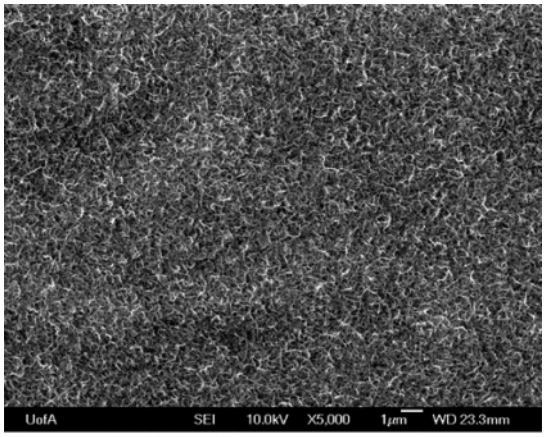

(a) Co: Mn = 3:1

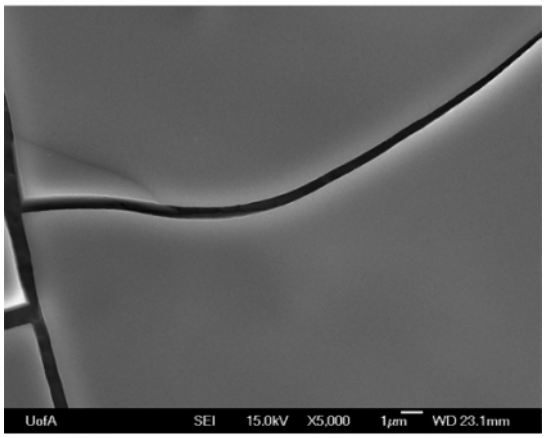

(b) Co: Mn = 59:1

Figure 6. Plan view SEM images of Mn−Co−O coatings prepared from solutions with two Co:Mn ratios at 70 °C. (a) Co:Mn = 3:1 and (b) Co:Mn = 59:1. The deposition current density was 5 mA/cm^2.

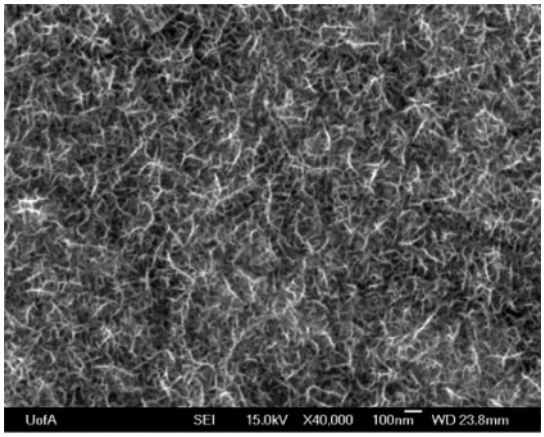

(a)

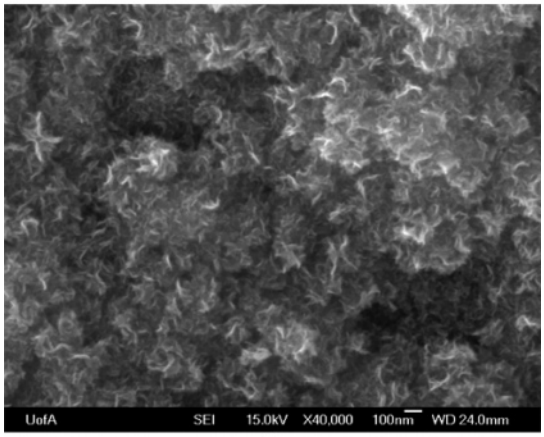

(b)

Figure 7. High-magnification plan view SEM images of typical Mn−Co−O coatings with and without cracks. (a) Co:Mn = 9:1, T = 50 °C, and i = 5 mA/cm^2 (with cracks). (b) Co:Mn = 9:1, T = 90 °C ,and i = 5 mA/cm^2 (without cracks).

ratio was 9:1. Cobalt content increases first with increasing current density and reaches a maximum value at 30mA/cm^2; Co content then decreases with any further increase in current density to 50 mA/cm^2. From the LSV spectra in Figure 2, it is apparent that the Mn oxides deposit at lower potentials than Co oxides. The cobalt content increases initially with increasing current density to a maximum value and then decreases when the applied overpotential surpasses the potential corresponding to the limiting current of the Co oxides.

To summarize, the composition of Mn−Co−O coatings can be successfully controlled by adjusting the deposition parameters.

Deposit Morphology. Figure 4 shows plan view SEM secondary electron (SE) images of Mn−Co−O coatings prepared from a 0.27 M $CoSO_4$ + 0.03 M $MnSO_4$ solution at two temperatures (50 and 90 °C). Cracks are distributed homogeneously on the surface for samples prepared at temperatures less than 50 °C. For samples prepared at higher temperatures, such as 70 and 90 °C, cracks are not present. Increasing the solution temperature also results in an increase in the coating oxide particle size.

Figure 5 shows plan view SE morphologies of Mn−Co−O coatings prepared from a 0.27 M $CoSO_4$ + 0.03 M $MnSO_4$ solution at 70 °C at two current densities (5 and 50 mA/cm^2). A high current density (50 mA/cm^2) can also induce crack formation in the coatings, even at elevated temperatures. Increasing the deposition current density leads to a reduction in the surface roughness.

The Mn−Co−O coating morphology prepared from solutions with two different Co:Mn ratios can be seen in Figure 6. A higher solution Co:Mn ratio results in smoother surfaces, but also a higher possibility of crack formation.

On the basis of Figures 4−6, crack formation is indeed influenced by solution temperature, solution concentration, and current density. Cracks are more likely to form in coatings with smooth surfaces. To clarify the morphology difference in coatings with and without cracks, SEM images of typical coatings were obtained at higher magnification (40 000×), as shown in Figure 7. The surface morphology is similar for the two SE images; the major difference is that the coating prepared from the solutions at higher temperature (without cracks) is more porous than the coating prepared from the solutions at lower temperature (with cracks). Therefore, porosity in the as-deposited Mn−Co−O coatings is likely one factor involved in crack formation.

Crystallization and Phase Information. Deposited films were examined using thin film XRD; the patterns had broad and weak diffracted peaks (not shown here), indicating that the as-deposited Mn−Co−O coatings are either amorphous or contain extremely small crystallites. To clarify the coating structure, the as-deposited coatings were analyzed using

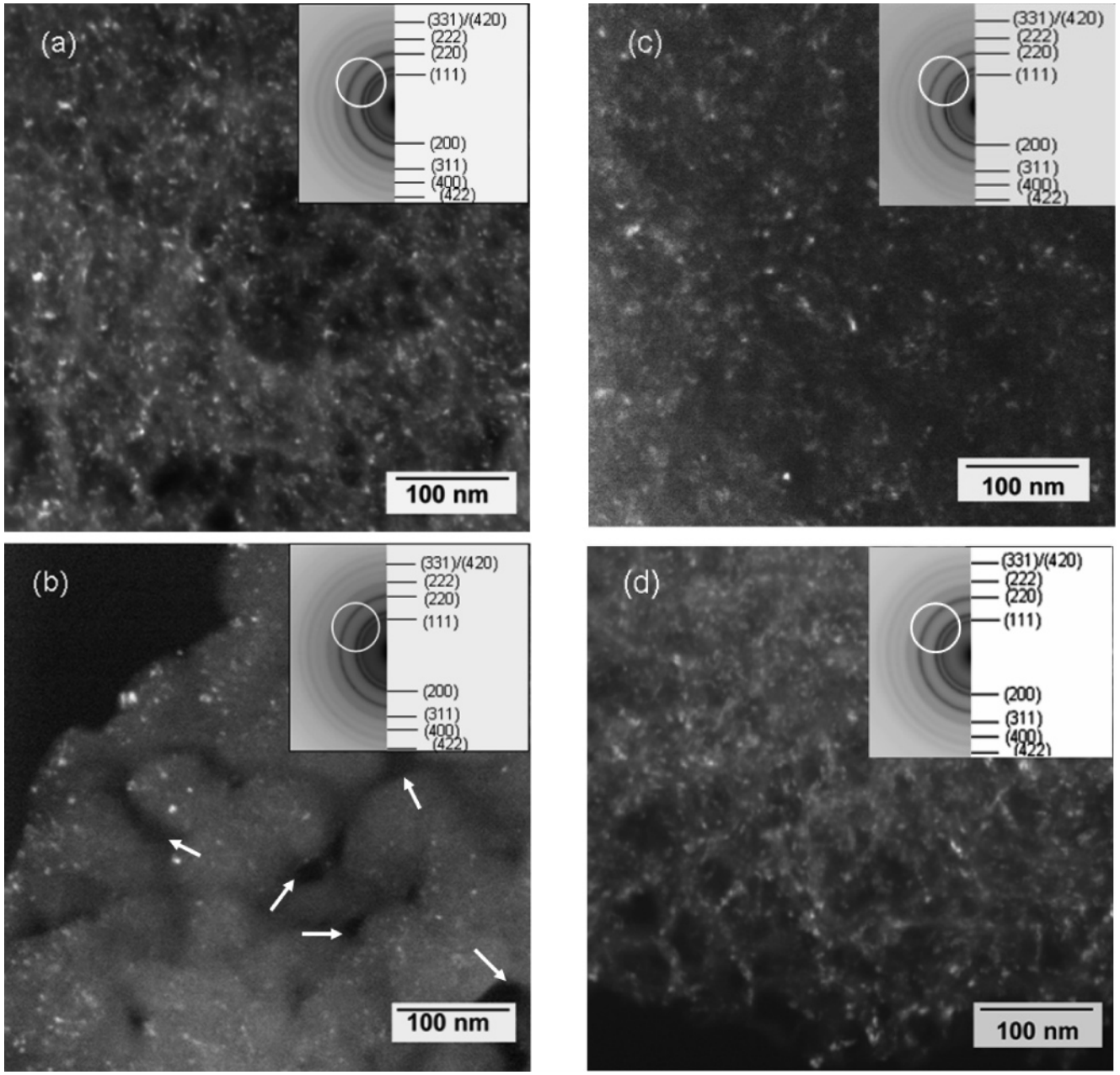

Figure 8. Representative dark-field TEM images and SAD patterns (inset) of Mn−Co−O coatings prepared under different conditions. (a) Co:Mn = 9:1, T = 50 °C, and i = 5mA/cm^2 (with cracks). (b) Co:Mn = 9:1, T = 90 °C, and i = 5mA/cm^2 (without cracks). (c) Co:Mn = 29:1, T = 70 °C, and i = 5 mA/cm^2 (higher Co content and no cracks). (d) Co:Mn = 9:1, T = 70 °C, and i = 50 mA/cm^2 (with cracks). The dark-field TEM images were taken from circled areas in the corresponding diffraction patterns.

TEM. Figure 8 shows representative dark-field (DF) TEM images and electron diffraction patterns of as-deposited Mn−Co−O coatings prepared under different deposition conditions. The DF TEM images were taken from part of the diffraction rings (circled areas in the corresponding diffraction patterns of Figure 8). Similar diffraction patterns were found for all coatings; these were fairly broad and continuous. This is an indication that the coatings have a similar crystal structure and are composed of nanocrystalline oxide particles with a relatively narrow size distribution ranging from several nanometers to about 10 nm. In summary, the deposition parameters, including solution temperature, solution concentration, and current density, have little influence on the crystal structure of as-deposited Mn−Co−O coatings.

Taking the composition data (Figure 3), morphology (Figures 4−6), and structural information (Figure 8) into account, it is noted that crack formation in Mn−Co−O coatings does not depend on phase structure, grain size, or even coating composition. Comparing the DF images Figure 8a and 8b, many submicrometer-sized voids, shown with arrows in Figure 8b, are visible in the coating prepared at the higher solution temperature (90 °C), which is consistent with Figure 7. The presence of these submicrometer-sized voids, i.e., microcracked zones, is expected to reduce the buildup of residual stress that gives rise to crack propagation.[31] Further study is needed to elucidate how deposition

(31) Green, D. J. *An Introduction to Mechanical Properties of Ceramics*; Cambridge University Press: Cambridge, UK, 1998; pp 258−260.

Table 1. Electron Diffraction Information for the As-Deposited Mn−Co−O Coatings

d-spacing (nm)				$(d_1/d_i)^2$ values rounded to nearest integer	*hkl*
a	*b*	*c*	*d*		
0.250	0.249	0.248	0.249	3	(111)
0.214	0.213	0.212	0.213	4	(200)
0.151	0.151	0.150	0.150	8	(220)
0.130	0.129	0.128	0.129	11	(311)
0.123	0.123	0.122	0.122	12	(222)
0.108	0.106	0.106	0.106	16	(400)
0.096	0.096	0.095	0.095	19/20	(331)/(420)
0.087	0.087	0.086	0.086	24	(422)

conditions affect the submicrometer-sized void formation and subsequent crack formation in as-deposited Mn−Co−O coatings.

Careful examination of the SAD patterns in Figure 8 reveals a total of eight characteristic diffraction rings. The experimental interplanar distances determined from these rings are given in the first four columns in Table 1. The *d*-spacings and intensities of these rings were compared with those of stable Mn−Co−O spinel oxides from the X-ray diffraction database;[32] no match was obtained. The $(d_1/d_i)^2$ values were calculated and are shown in Table 1, rounded to the nearest integer. These SAD patterns show systematic absences to be consistent with those of a face-center cubic (FCC) structure, and the possible diffraction planes are listed in Table 1. The diffraction rings related to (331) and (420) planes are too close to be distinguishable in the SAD patterns, so the two planes are listed together. It can be concluded that the as-deposited Mn−Co−O coatings have a metastable FCC structure, which is quite different from the amorphous and hydrous Mn,[33] Co−Mn,[28] and Ni−Mn[29] oxides prepared by anodic electrodeposition, as described in earlier investigations. The lattice parameter was estimated to be $a = 0.426-0.428$ nm. The diffracted rings are labeled, based on an FCC structure, in the SAD patterns in Figure 8.

According to Figure 3, the four coatings in Figure 8 have Co contents ranging from 35 to more than 60%. However, the as-deposited crystal structure is not sensitive to the coating composition. This implies that Mn and Co cations are exchangeable in the metastable FCC unit cell. As Co content in the coatings increases, there is a slight decrease in the *d* spacings (Table 1). This decrease can be attributed to the smaller cation size for Co relative to Mn.[34] To uncover the nature of the phase formation of the as-deposited Mn−Co−O coatings, more microscopic work is needed.

Conclusions

Anodic electrodeposition has been applied to prepare Co-rich, nanocrystalline Mn−Co−O coatings without cracks on ferritic stainless steel substrates from aqueous solutions at high temperatures (≥70 °C). The chemistry and morphology of the coatings can be manipulated by adjusting deposition parameters, including solution temperature, metal ion concentration, and current density. Coating crack formation depends on deposition conditions, most notably current density and solution temperature, but is independent of crystal structure, grain size, and even coating composition. TEM analysis revealed that as-deposited Mn−Co−O coatings are composed of nanocrystalline oxide grains ranging from several nanometers to ten nanometers in diameter with a metastable face center cubic (FCC) structure. The crystal structure of as-deposited coatings is not sensitive to deposition parameters.

Acknowledgment. The authors are grateful to the Natural Sciences and Engineering Research Council (NSERC) of Canada and Versa Power Systems (VPS) for providing funding for this project.

CM070147Q

(32) *JCPDS*; International Center for Diffraction Data: Newtown Square, PA, 1996.
(33) Chang, J. K.; Tsai, W. T. *J. Electrochem. Soc.* **2005**, *152*, A2063−A2068.
(34) Shannon, R. D. *Acta Crystallogr., Sect. A* **1976**, *32*, 751−767.